QCD measurements in ATLAS

Javier Llorente

On behalf of the ATLAS Collaboration

SILAFAE 2016. November 14, 2016

Outline of the talk

- Motivation
- The ATLAS detector and object reconstruction
  - Jet reconstruction and calibration
  - Photon reconstruction and identification
- Jet measurements
  - Inclusive (1,2,3,4)-jet differential cross sections.
  - Production cross section for jets containing B-hadrons.
  - Jet substructure (jet shapes, jet charge, track multiplicity)
  - Global event properties (event shapes, jet vetoes and azimuthal decorrelations)
  - Measurements of the strong coupling (TEEC)
- Photon measurements
  - Isolated photon-pair production.
  - Dynamics of isolated photon+jet production
  - Inclusive isolated prompt photon production

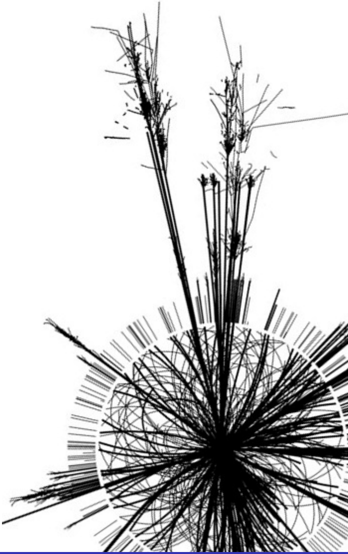

Motivation

There are several motivation items for measuring jet and photon observables and cross-sections:

- Testing QCD at large energy scales provided by the LHC.
- Evaluate the agreement of the data with fixed-order theoretical predictions.
- Evaluate the agreement of the data with parton shower Monte Carlo predictions.
- Extraction of Standard Model QCD parameters (α_s)
- Explore differences between parton flavours in jet substructure variables

Anatomy of a pp collision

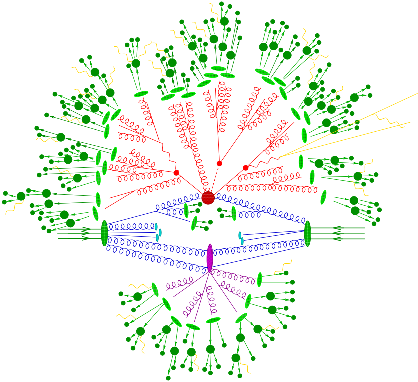

- Hard scattering: The main physics process under study (red spot).
- Underlying event: Additional (soft) hadronic activity due to multiparton interaction (purple spot).
- Parton shower: Emission of partons by QCD radiation (red).
- Hadronisation: Fragmentation of partons into hadrons (green).
- Pileup: Additional activity due to multiple *pp* collisions in a bunch crossing.

Correction for non-perturbative effects for an observable $\mathcal{O}$

$$C_{NP} = \frac{\mathcal{O}(\text{hadron level} + \text{UE})}{\mathcal{O}(\text{parton level, no UE})}$$

1. The ATLAS detector and object reconstruction

- Multi-purpose particle detector at the LHC
- Sampling calorimeters with high granularity (3 EM layers, 3 Had layers)
- High-efficiency jet and photon reconstruction

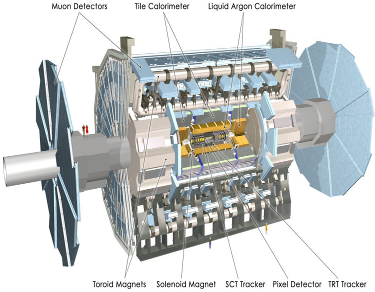

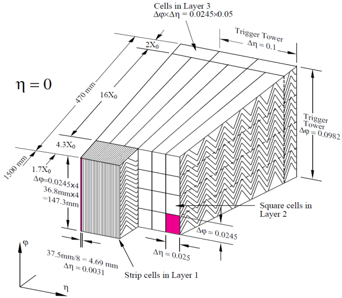

Jet reconstruction in ATLAS

Inputs to jet reconstruction: 3-Dimensional Topological Clusters.

- Iteratively constructed from calorimeter cells.
- Seeded from $|E| > 4\sigma$ cells. $|E| > 2\sigma$ cells and perimeter cells are added.
- Variable size.
- Aim to contain the shower from each hadron.

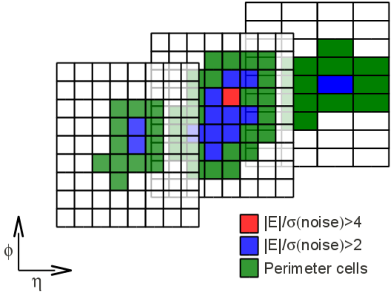

Jet algorithm: anti-k_T.

- Iterative algorithm based on the metric d_{ij}
- Infrared and collinear safe.
- Radius parameter $R = 0.4$.

$$\left.\begin{aligned} d_{ij} = \min\left(\frac{1}{k_{Ti}^2}, \frac{1}{k_{Tj}^2}\right)\frac{\Delta R_{ij}^2}{R^2} \\ d_{iB} = \frac{1}{k_{Ti}^2} \end{aligned}\right\}$$

The jet calibration follows a four-step procedure

- 1. Pileup correction: Subtraction of the offset from pileup as a function of N_{PV} and $\langle\mu\rangle$.
- 2. Origin correction: Correction of the jet direction to point to the primary interaction vertex.

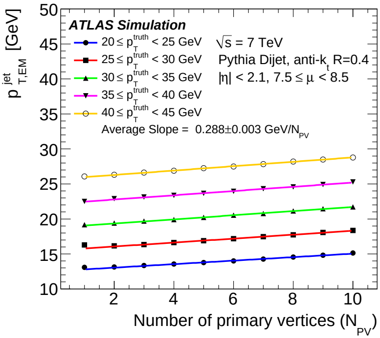

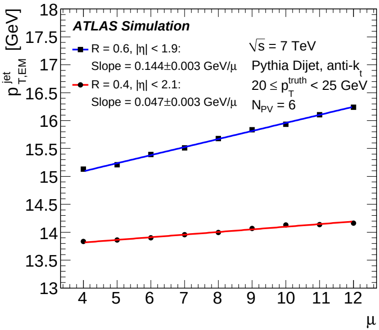

The jet calibration follows a four-step procedure

- 3. Energy calibration: The jet energy is corrected using simple correction factors derived from the MC
- 4. In situ corrections: The jet calibration is tested using different topologies (Z+jets, γ+jet, multijet...)

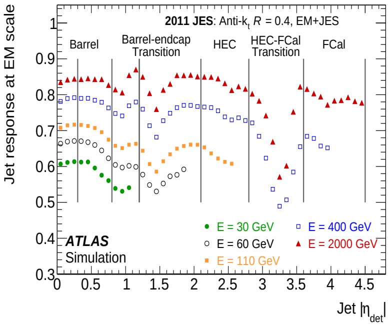

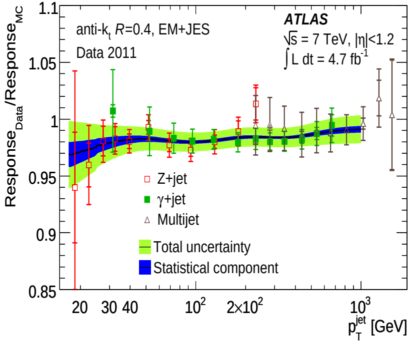

The identification of photons is based on 9 basic discriminating variables

- Hadronic leakage: The fraction of energy deposited in the hadronic calorimeter.
- Lateral shower shapes (Layer 2)

$$R_\eta = \frac{E_T^{3\times 7}}{E_T^{7\times 7}}; \quad R_\phi = \frac{E_T^{3\times 3}}{E_T^{3\times 7}}$$

- Lateral η-width RMS (Layer 2)

$$w_2 = \sqrt{\frac{\sum_c (E_c \times \eta_c^2)}{\sum_c E_c} - \left[\frac{\sum_c (E_c \times \eta_c)}{\sum_c E_c}\right]^2}$$

- $\pi^0 \to \gamma\gamma$ rejection: Study of the second maximum (Layer 1)

$$\Delta E_s = E_{\mathrm{max2}} - E_{\mathrm{min}}; \quad R_{\mathrm{max2}} = \frac{E_{\mathrm{max2}}}{(1 + 9 \times 10^{-3} E_T/\mathrm{GeV})}$$

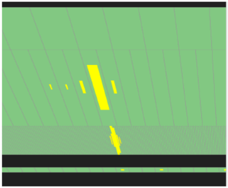

Unconverted γ

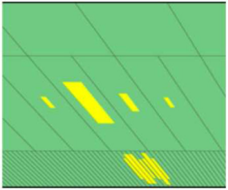

$\pi^0 \to \gamma\gamma$

Photon reconstruction and identification

The identification of photons is based on 9 basic discriminating variables

- F_{side}: The fraction of energy outside the core of three central strips in the first layer.
- w_{s3}: Shower width over three strips around the one with maximum energy

$$w_{s3} = \sqrt{\frac{\sum_i E_i (i - i_{\mathrm{max}})^2}{\sum_i E_i}}$$

- w_{stot}: The shower width over n strips, covering 2.5 cells of the second layer

These nine variables are used to define two photon qualities

- Loose: Hadronic leakage, R_η and w_2
- Tight: Tightened loose criteria, R_ϕ and shower shapes in the first layer ($\pi^0 \to \gamma\gamma$)

Photon reconstruction and identification

Distributions of shower shapes for signal (red) and backgrounds (black)

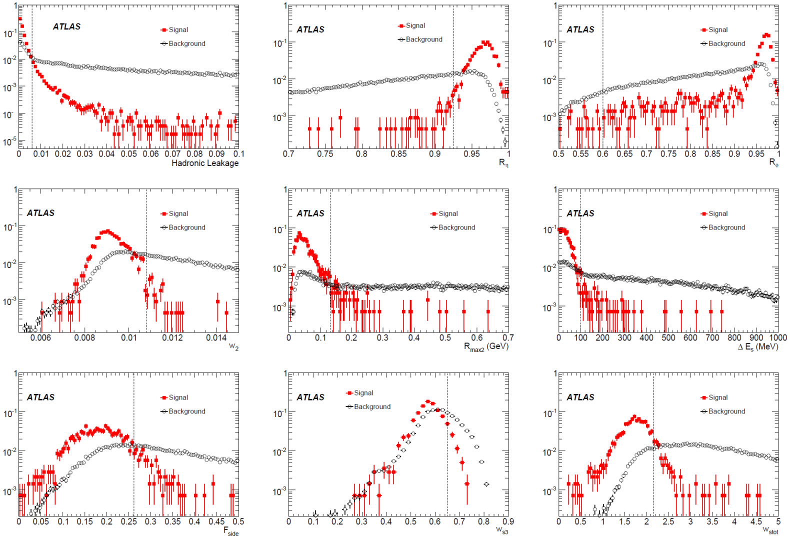

Identification efficiency for best quality ('tight') unconverted (top) and converted photons (bottom)

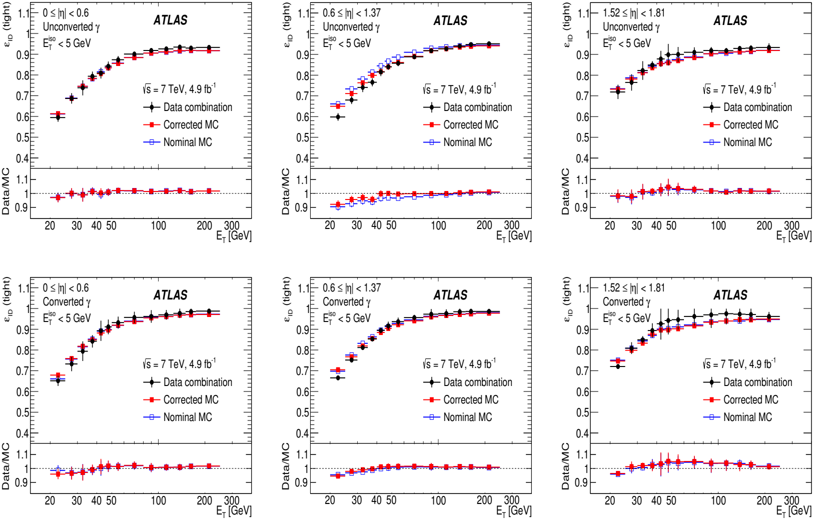

2. Jet measurements

- Double-differential cross section as a function of the jet p_T and rapidity. $\sqrt{s} = 7$ TeV, $\int Ldt = 4.5$ fb^{-1}.
- Jets kinematics: $p_T \geq 100$ GeV, $|y| < 3$.
- Comparison with NLO predictions corrected for EW and NP effects. Several PDFs investigated.

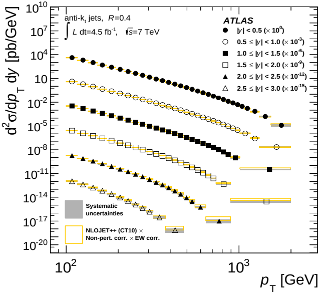

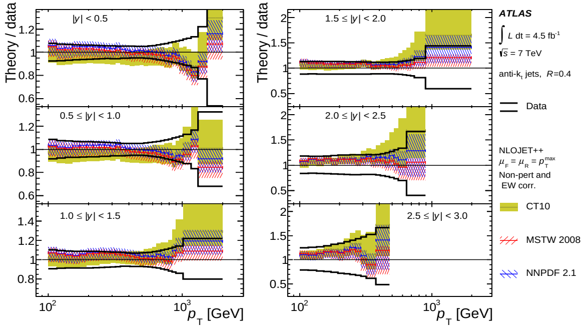

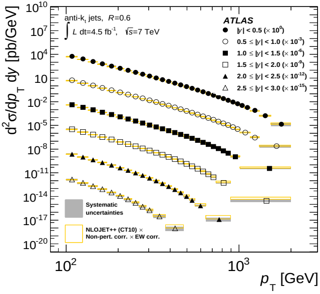

Experimental and theoretical uncertainties

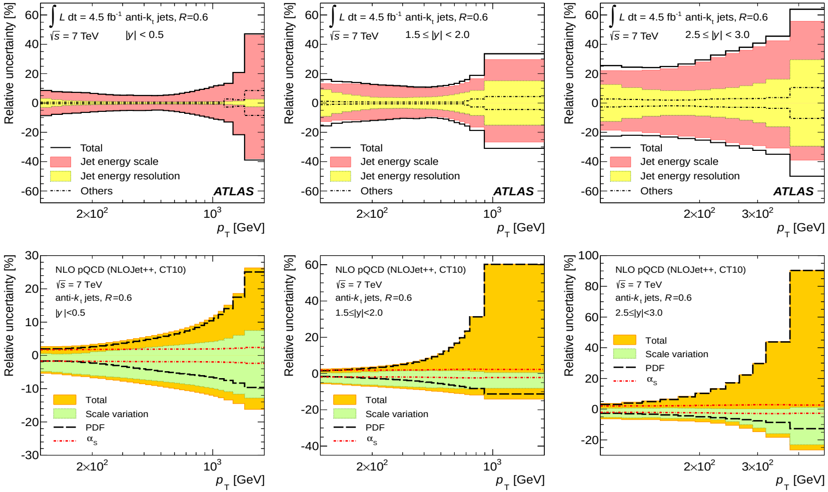

- JES dominates the experimental uncertainties.
- PDF dominates the theoretical uncertainties.

Inclusive jets at $\sqrt{s} = 7$ TeV. JHEP 02, 153 (2015)

Theoretical predictions at the parton level need to be corrected for non-perturbative effects (hadronisation + multiple parton interactions)

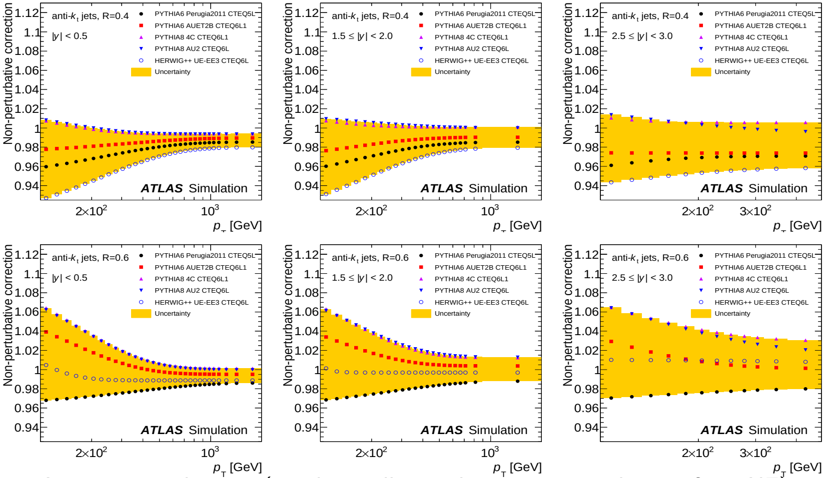

- Important at low p_T (jets less collimated, greater contribution from UE)
- Differences in $R = 0.4$ and $R = 0.6$ (different UE / Hadronisation effect)

- $p_T > 100$ GeV and $|y| < 3$
- Comparison with new-generation PDF sets CT14, MMHT2014, NNPDF 3.0, HERAPDF 2.0, ABM12

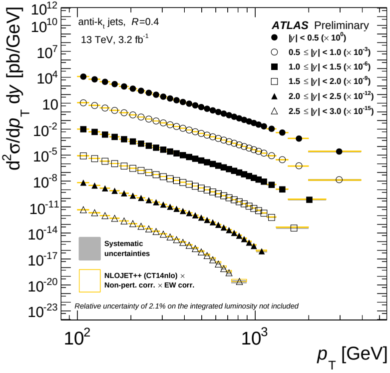

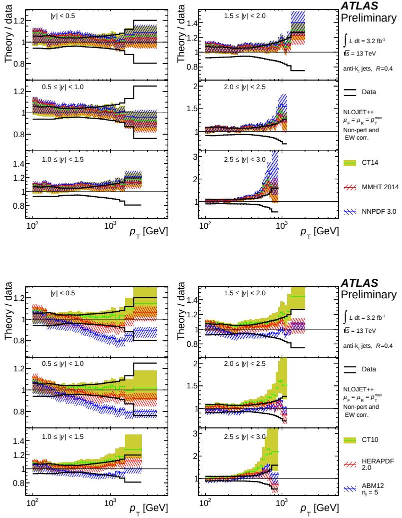

- Double-differential cross section as a function of m_{12} and $y^* = |y_1 - y_2|/2$. $\sqrt{s} = 7$ TeV, $\int Ldt = 4.5$ fb^{-1}.
- Kinematical requirements: $p_{T1} \geq 100$ GeV, $p_{T2} > 50$ GeV and $|y| < 3$
- Comparison with NLO predictions corrected for EW and NP effects. Several PDFs investigated.

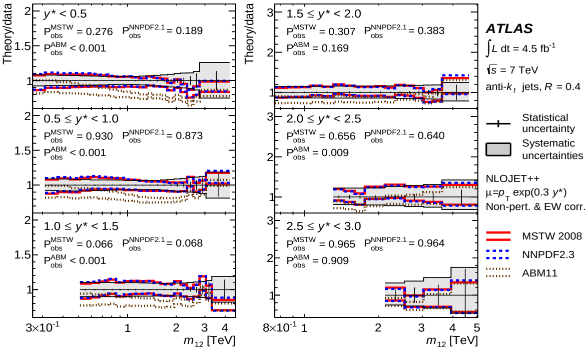

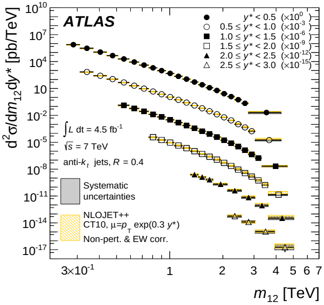

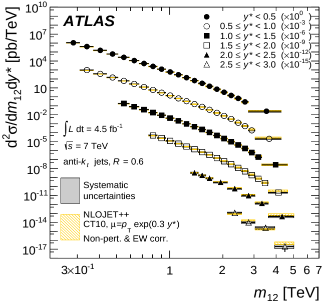

Non-perturbative and electroweak corrections

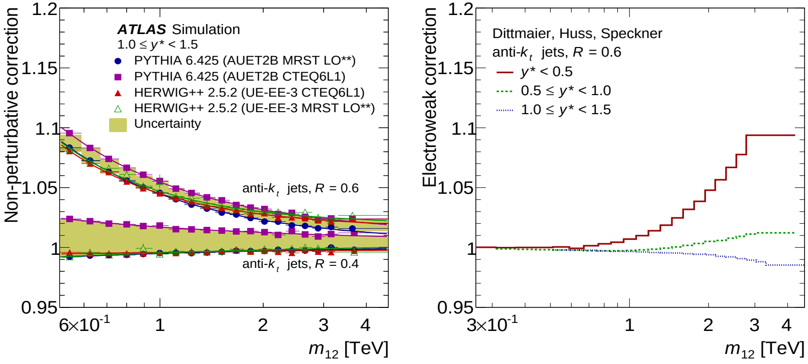

- Non-perturbative corrections are larger at low masses.
- Electroweak corrections are enhanced at high masses $\sim \alpha_W \log^2\left(\frac{Q^2}{M_W^2}\right)$ [Dittmaier, Huss, Speckner, JHEP 11 095 (2012)]

The agreement of the data with NLO pQCD predictions is tested using a χ^2 with asymmetric uncertainties.

$$\chi^2(d;t) = \min_{\beta_a} \left\{ \sum_{i,j} [d_i - F_i(\beta_a)] \left[C_{su}^{-1}(t) \right]_{ij} [d_j - F_j(\beta_a)] + \sum_a \beta_a^2 \right\}$$

$$F_i(\beta_a) = \left(1 + \sum_a \beta_a (\epsilon_a^{\pm}(\beta_a))_i \right) t_i$$

Contact interactions are excluded in the region $\Lambda < 7.1$ TeV.

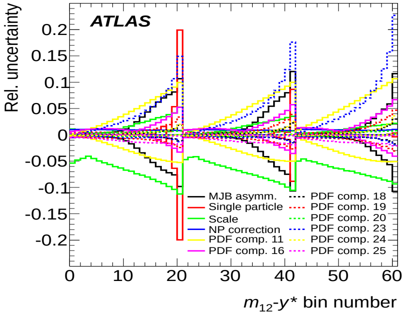

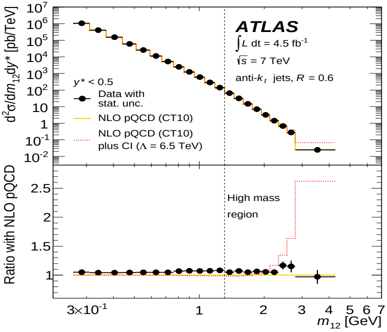

Three-jet cross sections at $\sqrt{s} = 7$ TeV. Eur. Phys. J. C 75 (2015)

- Double-differential cross section as a function of m_{jjj} and $|Y^*| = |y_1 - y_2| + |y_2 - y_3| + |y_1 - y_3|$. $\sqrt{s} = 7$ TeV, $\int Ldt = 4.5$ fb^{-1}.
- Asymmetric kinematics: $p_{T1} > 150$ GeV, $p_{T2} > 100$ GeV and $p_{T3} > 50$ GeV.
- NLO predictions corrected for NP effects. Several PDFs used.

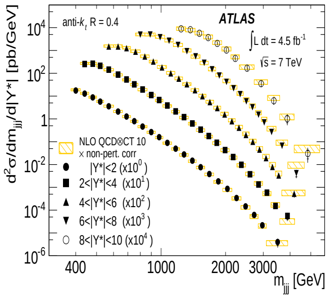

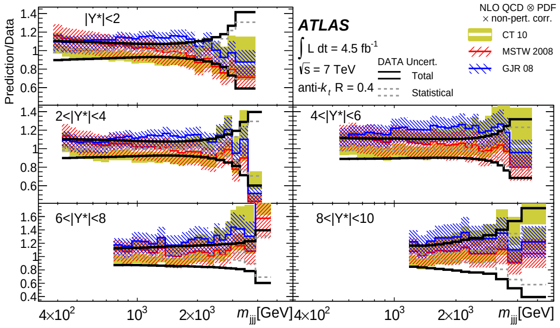

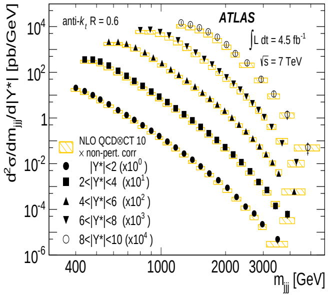

Experimental and theoretical uncertainties

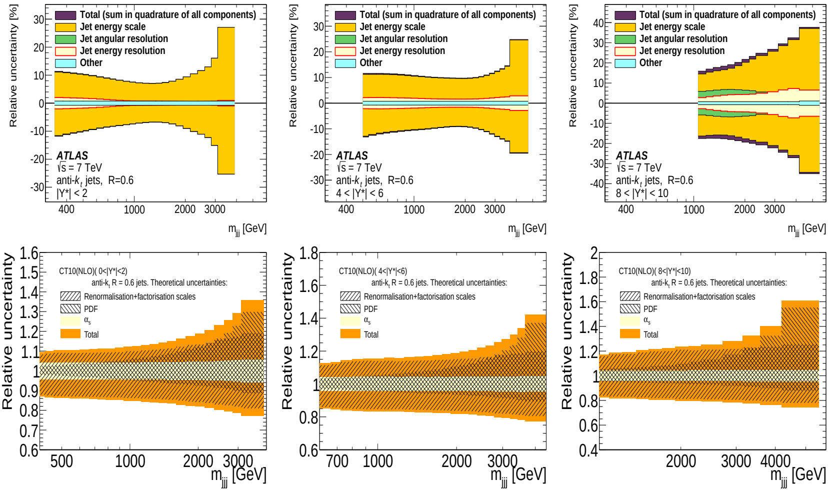

- JES dominates the experimental uncertainties.
- (μ_R, μ_F) dominates the theoretical uncertainties.

Non-perturbative corrections

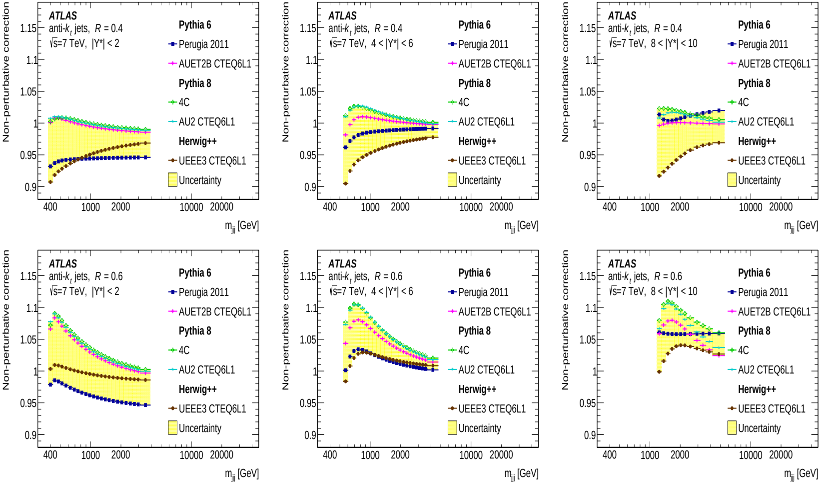

- Important at low masses m_{jjj}
- Differences in $R = 0.4$ and $R = 0.6$ (different UE / Hadronisation effect)

Four-jet cross sections at $\sqrt{s} = 8$ TeV. JHEP 12, 105 (2015)

- Wide variety of four-jet observables.
- Kinematics: $p_T^{(1)} > 100$ GeV, $p_T^{(2,3,4)} > 64$ GeV and $|\eta| < 2.8$. Separation $\min(\Delta R_{ij}) > 0.65$.
- NLO predictions by BlackHat and NJet + Sherpa. Comparison with HEJ also available.
- Correct description of the shapes by NLO pQCD and MadGraph+Pythia. $2 \to 2$ + PS gives a poor description.

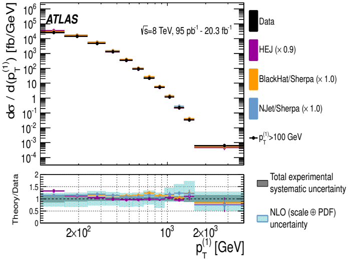

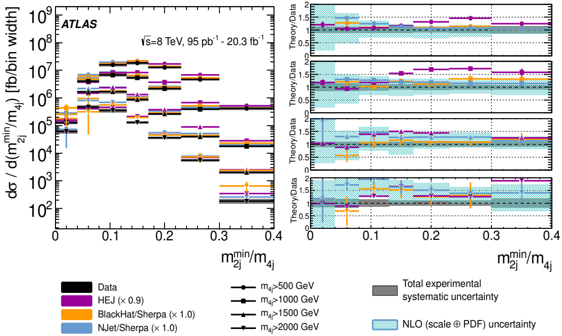

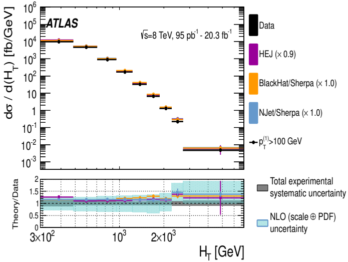

- Cross-section of $b\bar{b}$ pairs as a function of several dijet observables.
- Leading jet $p_T > 270$ GeV and $|\eta| < 3.2$. Two b-jets with $p_T > 20$ GeV, $|\eta| < 2.5$ and $\log(p_b/p_l) > 0.35$. Separated by $\Delta R > 0.4$.
- Suppression of flavour creation with respect to gluon splitting. MC fails to describe the data in regions not dominated by two hard b-jets.
- Bin-by-bin determination of the fraction of $b\bar{b}$ events using template fits.

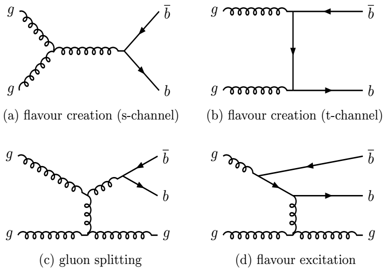

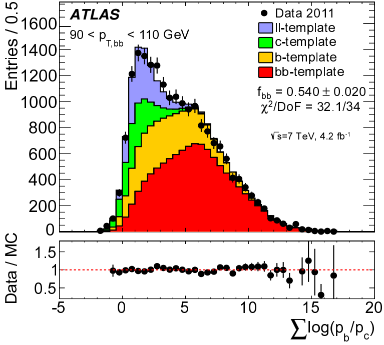

Differential cross-sections as a function of $p_{Tb\bar{b}}$ and $m_{b\bar{b}}$

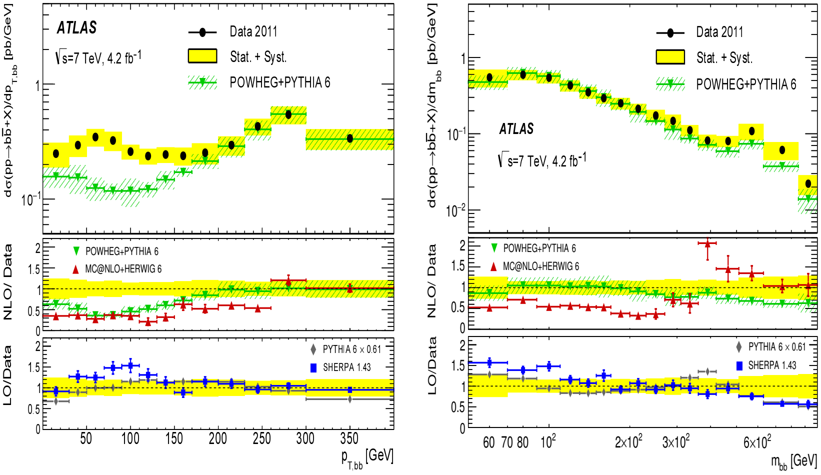

Differential cross-sections as a function of $\Delta\phi_{b\bar{b}}$ and $y^* = |y_b - y_{\bar{b}}|/2$

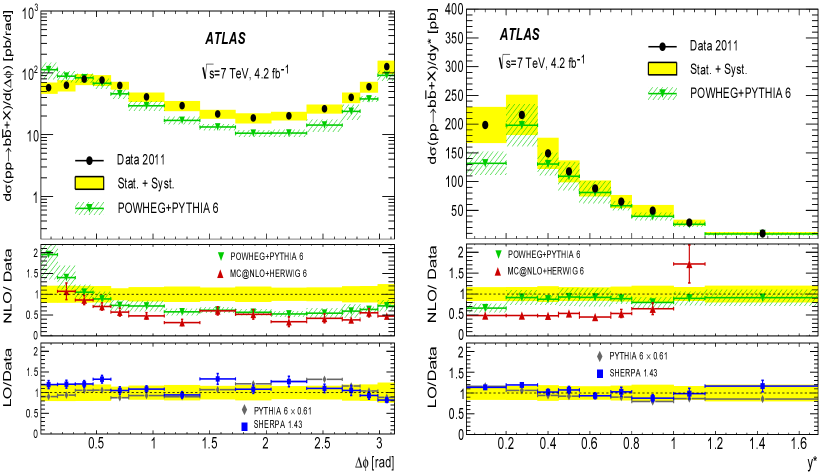

Jet shapes

- Normalised momentum flow as a function of the distance to the jet axis.
- Sensitive observables for the modelling of the parton shower.
- Sensitive to the different colour factors (quark / gluon couplings) and mass of the initiating parton (heavy vs light quarks)

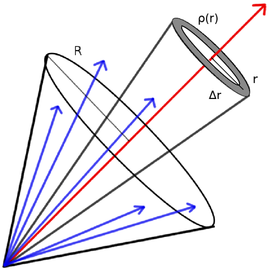

- Differential jet shape $r \leq R - \Delta r/2$

$$\rho(r) = \frac{1}{\Delta r}\frac{p_T(r-\Delta r/2, r+\Delta r/2)}{p_T(0,R)}$$

- Integrated jet shape $r \leq R$

$$\Psi(r) = \frac{p_T(0,r)}{p_T(0,R)}$$

Differential and integrated jet shapes ($R = 0.6$) binned for several p_T regimes

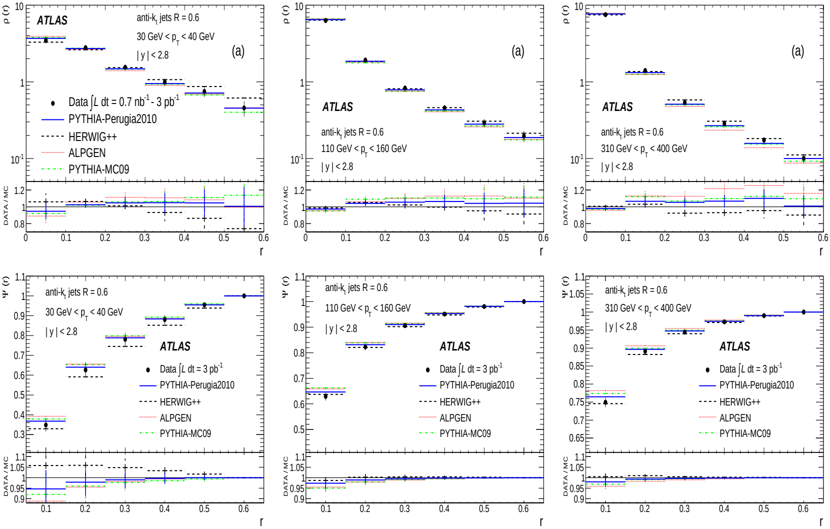

Larger p_T ⇒ more collimated jets (greater ρ for small r)

Value of $1 - \Psi(r = R/2)$ as a function of p_T

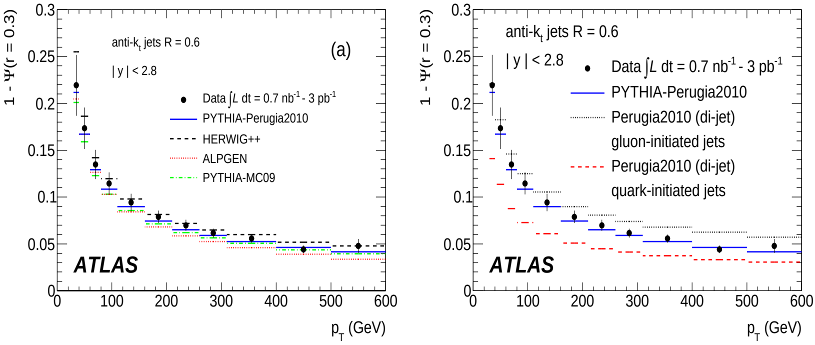

- Good description by the Monte Carlo expectations.
- Crucially dependent on the flavour of the initiating parton
- Quark jets are more collimated due to smaller colour factor on qg vertices

Dead cone effect: The gluon emission off a quark crucially depends on its mass ($\theta_0 = m_q/E_q$) [Dokshitzer, Khoze and Troyan, J. Phys. G 17 1602 (1991)]

$$\left(\frac{d\sigma}{d\omega}\right)_{q\to\tilde{q}g} = \frac{\alpha_s C_F}{\pi\omega}\frac{(2\sin\theta/2)^2 d(2\sin\theta/2)^2}{[(2\sin\theta/2)^2+\theta_0^2]^2}\left[1+\mathcal{O}(\theta_0,\omega)\right] \sim \frac{1}{\omega}\frac{\theta^2 d\theta^2}{[\theta^2+\theta_0^2]^2}$$

Two samples of jets are selected, attending to flavour

- b-jets from $t \to Wb$ decays
- Light jets (u, d, c, s) from $W \to q\bar{q}'$ decays

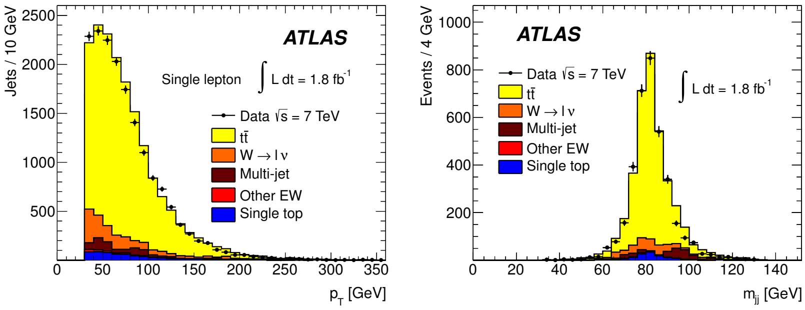

- Clear difference between jets initiated by light and *b*-quarks
- Effect less pronounced at high p_T
- Good description by NLO + PS Monte Carlos (MC@NLO, Powheg)

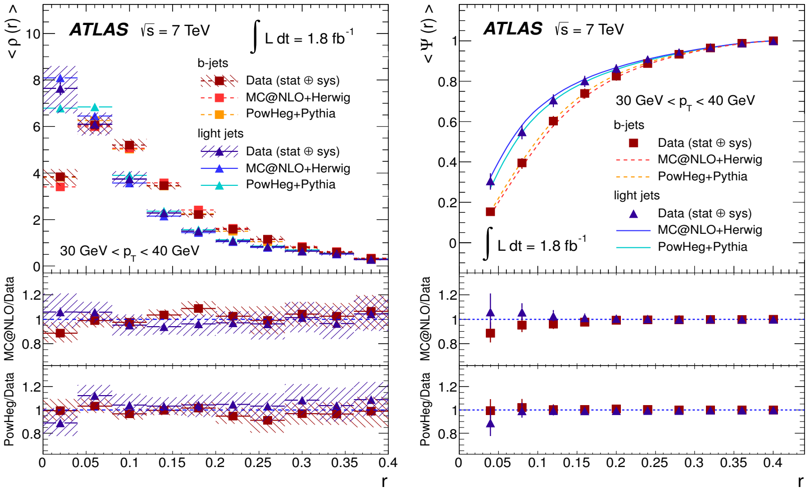

Jet shapes in $t\bar{t}$ events. Eur. Phys. J. C 73, 2676 (2013)

Input for determination of the *b*-quark mass [Llorente, Cantero, NPB 889, 401 (2014)]

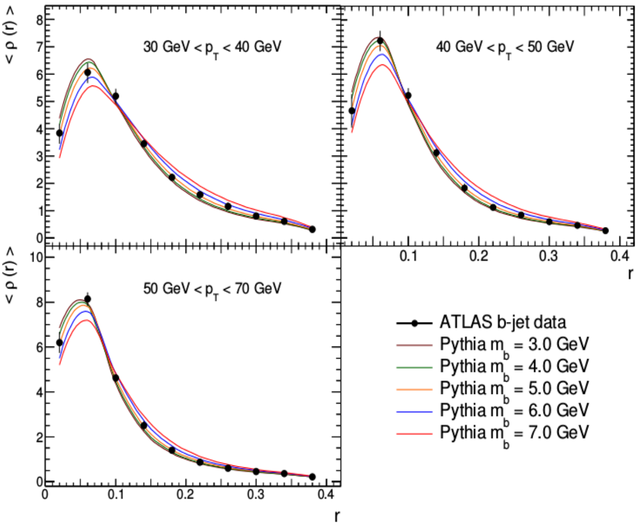

$$m_b = 4.86 \pm 0.08\ (\text{exp.})\ \pm 0.39\ (\text{Gen.})\ ^{+0.02}_{-0.01}\ (\text{ISR})\ ^{+0.18}_{-0.00}\ (\text{FSR})\ ^{+0.17}_{-0.00}\ (\text{CR})\ ^{+0.14}_{-0.13}\ (\Lambda_s)\ \text{GeV}$$

Jet charge defined as a sum over the charged particles within a jet

$$Q = \frac{\sum_i q_i (p_T^i)^\kappa}{(p_T^{\mathrm{jet}})^\kappa}$$

- Jet selection: $p_T > 50$ GeV and $|\eta| < 2.1$. p_T-balance: $p_T^{(1)}/p_T^{(2)} < 1.5$
- κ regulates the sensitivity of Q to the soft radiation

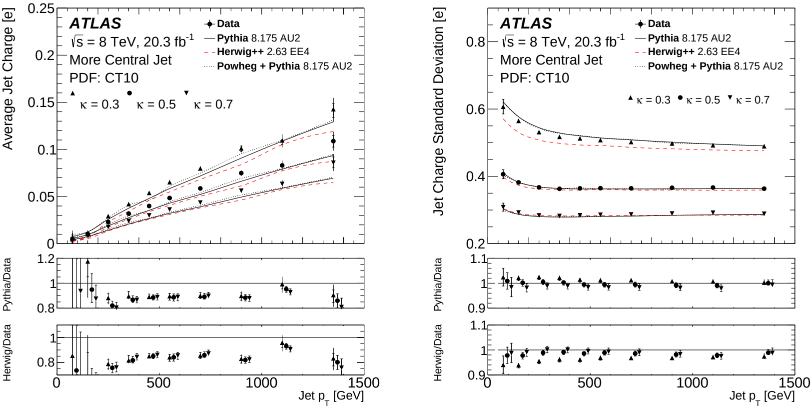

These measurements are sensitive to the quark charges Q_u and Q_d

$$\left.\begin{array}{c}\langle Q_{J,i}^{\text{forward}}\rangle = (f_{u,i}^{\text{forward}} - f_{\bar{u},i}^{\text{forward}})Q_u + (f_{d,i}^{\text{forward}} - f_{\bar{d},i}^{\text{forward}})Q_d \\ \langle Q_{J,i}^{\text{central}}\rangle = (f_{u,i}^{\text{central}} - f_{\bar{u},i}^{\text{central}})Q_u + (f_{d,i}^{\text{central}} - f_{\bar{d},i}^{\text{central}})Q_d\end{array}\right\}$$

The scaling parameter c_κ parameterising the dependence of $\langle Q\rangle$ with the jet p_T is also extracted

$$\langle Q_i\rangle(p_T) \simeq \sum_f \alpha_{f,i}\bar{Q}_f \left[1 + c_\kappa \log\left(\frac{p_{T,i}}{\bar{p}_T}\right)\right] + \mathcal{O}(c_\kappa^2)$$

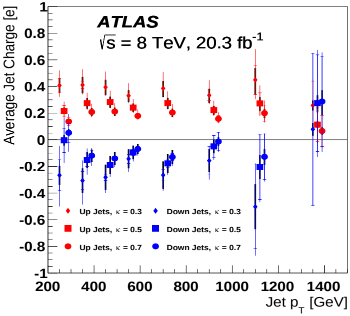

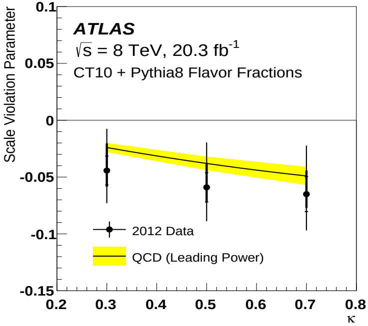

Same event selection as in $Q_{\rm jet}$ measurement. Measurement of the track multiplicity as a function of jet p_T ($Q_{\rm jet}$ with $\kappa = 0$)

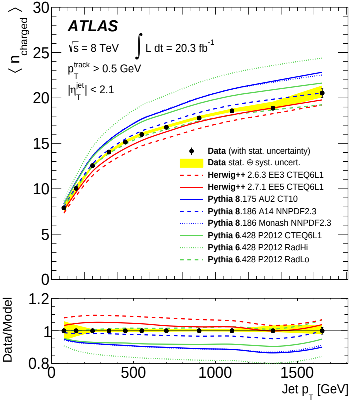

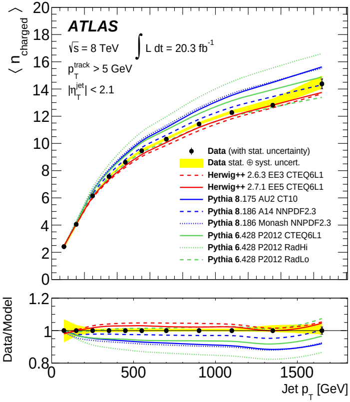

Different p_T cuts investigated for charged particles

Differences between forward and central jets are investigated. The quark and gluon multiplicities are also extracted

$$\left.\begin{aligned} \langle n^{\mathrm{f}}_{\mathrm{charged}}\rangle &= f^{f}_{g}\langle n^{g}_{\mathrm{charged}}\rangle + f^{f}_{q}\langle n^{q}_{\mathrm{charged}}\rangle \\ \langle n^{\mathrm{c}}_{\mathrm{charged}}\rangle &= f^{c}_{g}\langle n^{g}_{\mathrm{charged}}\rangle + f^{c}_{q}\langle n^{q}_{\mathrm{charged}}\rangle \end{aligned}\right\}$$

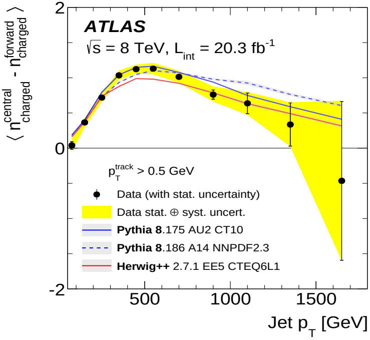

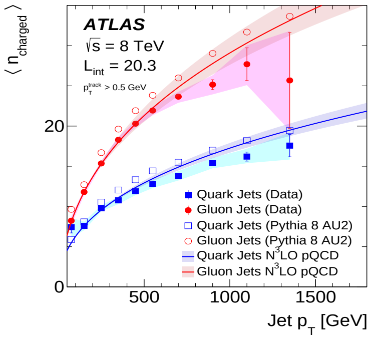

Measurement of observables sensitive to the geometrical distribution of QCD radiation

- Transverse Thrust and Transverse Minor are a measure of how linearly distributed is the energy on an event, with respect to the thrust axis $\hat{n}_T$

$$\tau_\perp = 1 - \max_{\hat{n}_T} \frac{\sum_i |\vec{p}_{T,i} \cdot \hat{n}_T|}{\sum_i p_{T,i}}; \quad T_{m,\perp} = \frac{\sum_i |\vec{p}_{T,i} \times \hat{n}_T|}{\sum_i p_{T,i}}$$

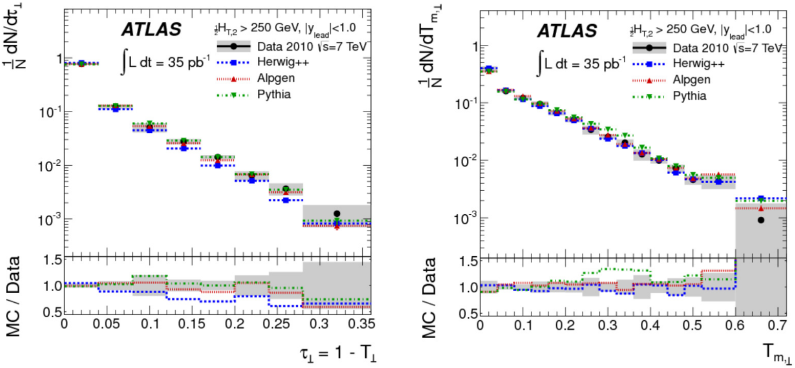

- The sphericity is a measure of how homogeneous is the energy distribution

$$S_{\alpha\beta} = \frac{\sum_i p_{\alpha,i} p_{\beta,i}}{\sum_i |\vec{p}_i|^2} \Rightarrow \tilde{S} = \frac{1}{\sum_i |\vec{p}_i|^2} \sum_i \begin{pmatrix} p_{x,i}^2 & p_{x,i}p_{y,i} & p_{x,i}p_{z,i} \\ p_{y,i}p_{x,i} & p_{y,i}^2 & p_{y,i}p_{z,i} \\ p_{z,i}p_{x,i} & p_{z,i}p_{y,i} & p_{z,i}^2 \end{pmatrix}$$

- Sphericity scalars constructed from eigenvalues $\lambda_1 \geq \lambda_2 \geq \lambda_3$

$$S = \frac{3}{2}(\lambda_2 + \lambda_3); \quad S_\perp = \frac{2\lambda_2}{\lambda_1 + \lambda_2}$$

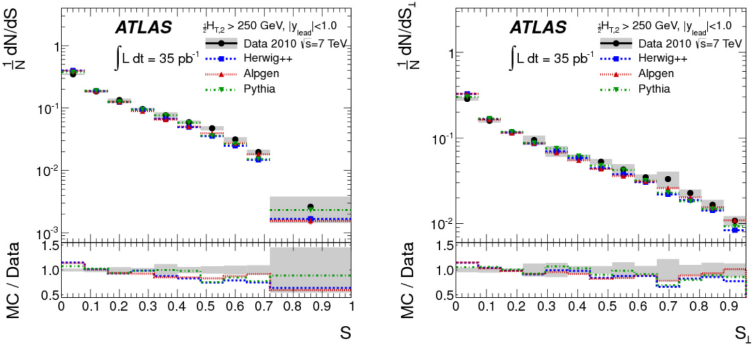

Event shapes at large Q^2 [Eur. Phys. J. C 72, 2211 (2012)]

- Aplanarity is a measure of the out-of-plane radiation

$$A = \frac{3}{2}\lambda_3$$

- Relative p_T of the third jet with respect to the two leading jets

$$y_{23} = \frac{p_{T3}^2}{(p_{T1} + p_{T2})^2}$$

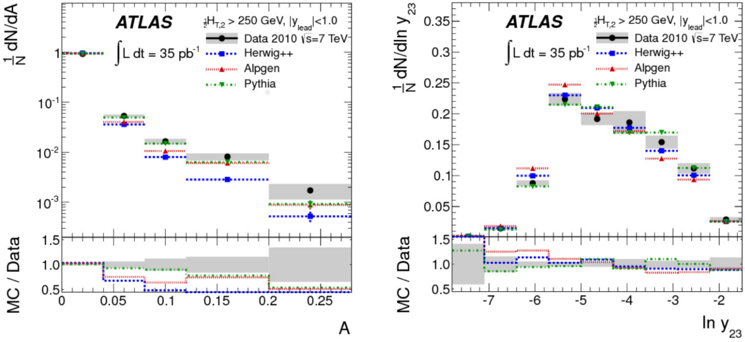

- Several observables measured, and their dependence on rapidity gap $\Delta y = y_1 - y_2$ and average transverse momentum $\overline{p_T} = \frac{1}{2}(p_{T1} + p_{T2})$
  - Gap fraction $\sigma_{jj}(Q_0)/\sigma_{jj}$ (fraction of events with no third jet with $p_T > Q_0$)
  - Average jet multiplicity, $\langle N_{jet} \rangle$, in rapidity gap between the two leading jets
  - $\langle cos(\pi - \Delta\phi) \rangle$ with $\Delta\phi$ the azimuth between the two leading jets.
- Kinematics: $p_{T1} > 60$ GeV, $p_{T2} > 50$ GeV for the dijet system.
- Sensitive to BFKL dynamics for large Δy.
- Comparisons with POWHEG and HEJ.

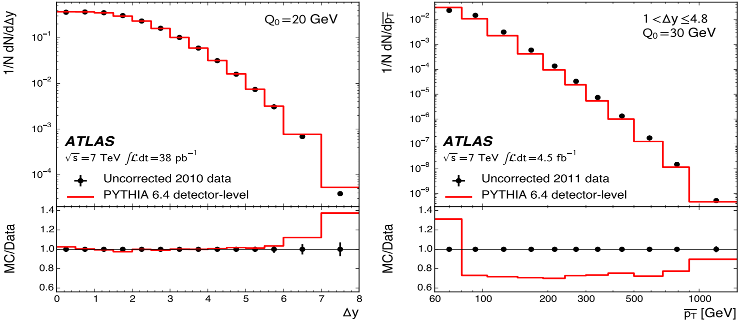

- Larger $\Delta y \Rightarrow$ More jet activity beyond Q_0 ($f(Q_0)$ decrease)
- Larger $\Delta y \Rightarrow$ More decorrelation (smaller $\Delta\phi$, $\langle\cos(\pi - \Delta\phi_{jj})\rangle$ decrease)

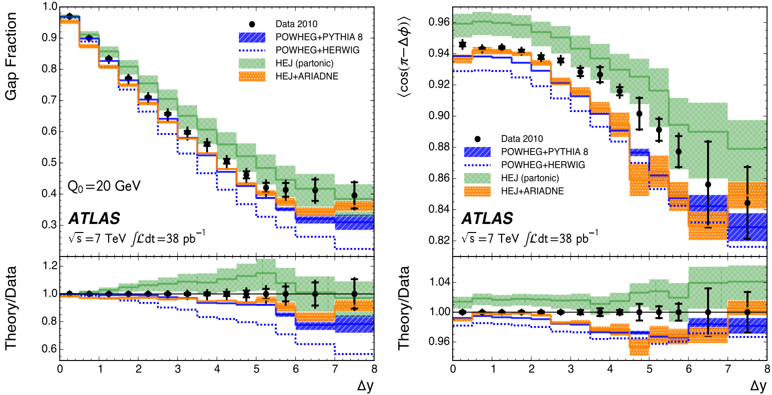

- Larger $\overline{p_T} \Rightarrow$ More jet activity beyond Q_0 ($f(Q_0)$ decrease)
- Larger $\overline{p_T} \Rightarrow$ Less decorrelation (larger $\Delta\phi$, $\langle\cos(\pi - \Delta\phi_{jj})\rangle$ increase)

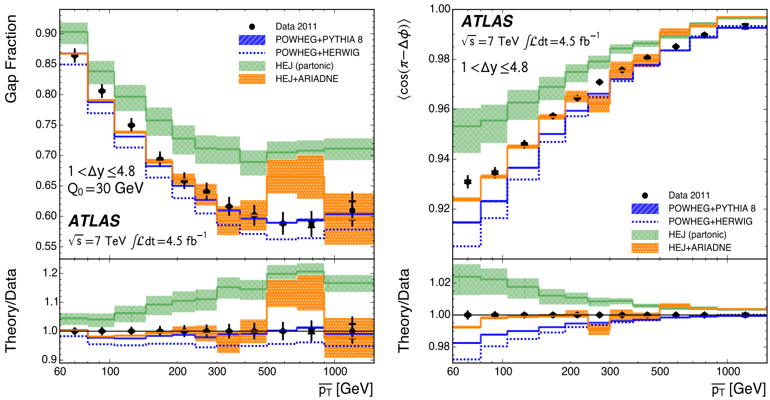

TEEC: The x_{T}-weighted distribution of differences in azimuth between jets i and j, with $x_{\mathrm{T}i} = \frac{E_{\mathrm{T}i}}{\sum_k E_{\mathrm{T}k}}$

$$\frac{1}{\sigma}\frac{d\Sigma}{d(\cos\phi)} = \frac{1}{\sigma}\sum_{ij}\int \frac{d\sigma}{dx_{\mathrm{T}i}dx_{\mathrm{T}j}d(\cos\phi)} x_{\mathrm{T}i}x_{\mathrm{T}j}dx_{\mathrm{T}i}dx_{\mathrm{T}j}$$

And the azimuthal asymmetry ATEEC is defined as

$$\frac{1}{\sigma}\frac{d\Sigma^{\mathrm{asym}}}{d(\cos\phi)} \equiv \frac{1}{\sigma}\frac{d\Sigma}{d(\cos\phi)}\bigg|_{\phi} - \frac{1}{\sigma}\frac{d\Sigma}{d(\cos\phi)}\bigg|_{\pi-\phi}$$

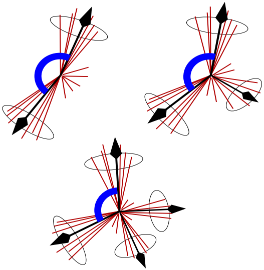

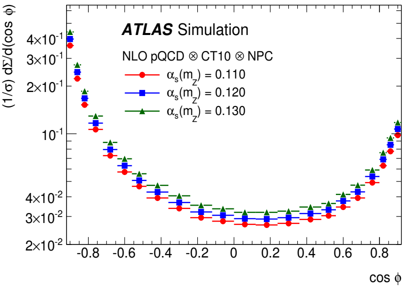

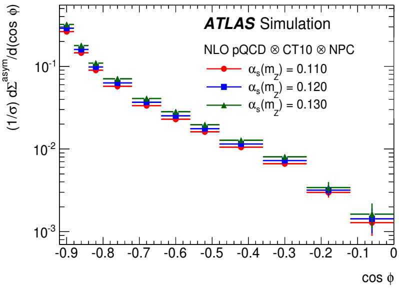

Good agreement with PYTHIA and ALPGEN expectations. HERWIG++ needs further tuning

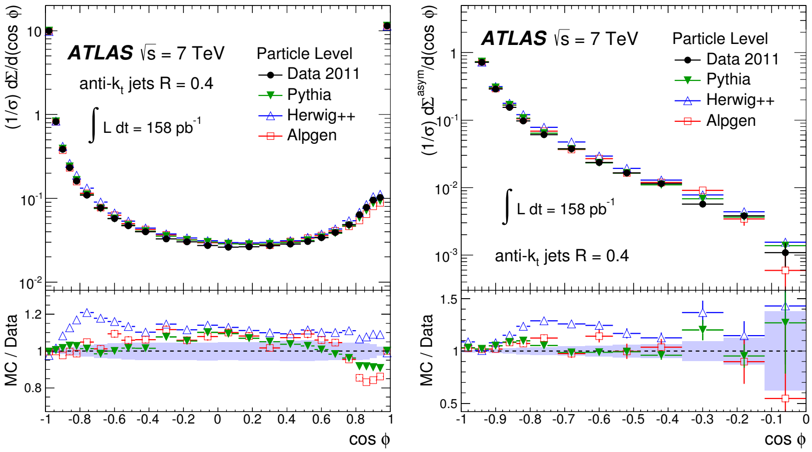

Transverse energy-energy correlations. Phys. Lett. B 750 427 (2015)

Very good agreement with pQCD predictions for $\alpha_s = 0.1180$ (CT10 PDF)

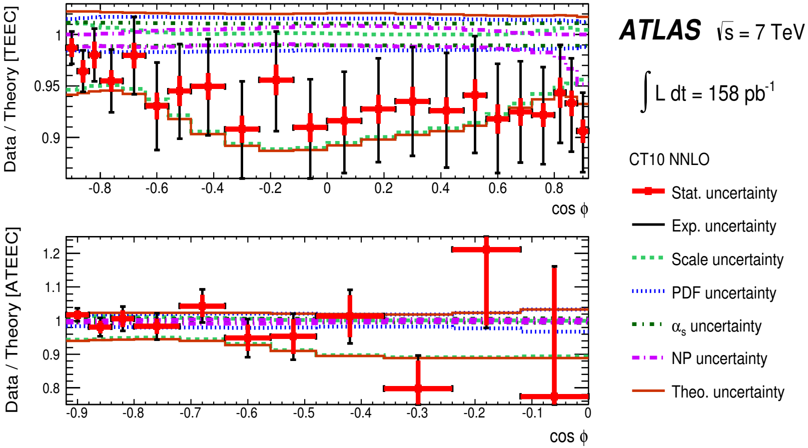

Fit to theoretical predictions using a χ^2 function with correlations between sources of uncertainty in order to determine α_s

$$\chi^2(\alpha_s,\vec{\lambda}) = \sum_i \frac{(x_i - F_i(\alpha_s,\vec{\lambda}))^2}{\Delta x_i^2 + \Delta\tau_i^2} + \sum_k \lambda_k^2 \; ; \text{ where } \; F_i(\alpha_s,\vec{\lambda}) = \psi_i(\alpha_s)\left(1 + \sum_k \lambda_k \sigma_k^{(i)}\right)$$

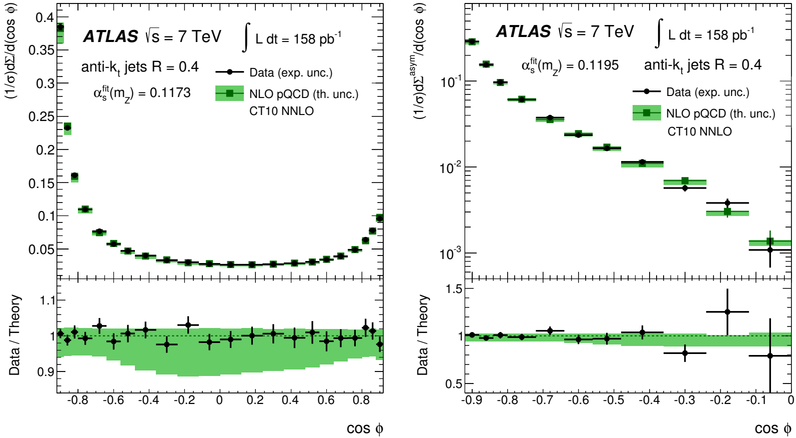

Transverse energy-energy correlations. Phys. Lett. B 750 427 (2015)

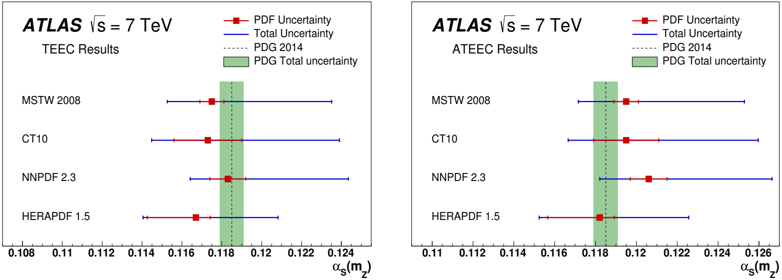

PDF	$\alpha_s(m_Z)$ value (TEEC fit)	χ^2/N_{dof}
MSTW 2008	0.1175 ± 0.0010 (exp.) $^{+0.0059}_{-0.0019}$ (scale) ± 0.0006 (PDF) ± 0.0002 (NPC)	29.0 / 21
CT10	0.1173 ± 0.0010 (exp.) $^{+0.0063}_{-0.0020}$ (scale) ± 0.0017 (PDF) ± 0.0002 (NPC)	28.4 / 21
NNPDF 2.3	0.1183 ± 0.0010 (exp.) $^{+0.0059}_{-0.0013}$ (scale) ± 0.0009 (PDF) ± 0.0002 (NPC)	29.3 / 21
HERAPDF 1.5	0.1167 ± 0.0007 (exp.) $^{+0.0040}_{-0.0008}$ (scale) $^{+0.0007}_{-0.0024}$ (PDF) ± 0.0001 (NPC)	28.7 / 21

PDF	$\alpha_s(m_Z)$ value (ATEEC fit)	χ^2/N_{dof}
MSTW 2008	0.1195 ± 0.0017 (exp.) $^{+0.0055}_{-0.0015}$ (scale) ± 0.0006 (PDF)	12.7 / 10
CT10	0.1195 ± 0.0018 (exp.) $^{+0.0060}_{-0.0015}$ (scale) ± 0.0016 (PDF)	12.6 / 10
NNPDF 2.3	0.1206 ± 0.0018 (exp.) $^{+0.0057}_{-0.0013}$ (scale) ± 0.0009 (PDF)	12.2 / 10
HERAPDF 1.5	0.1182 ± 0.0013 (exp.) $^{+0.0041}_{-0.0008}$ (scale) $^{+0.0007}_{-0.0025}$ (PDF)	12.1 / 10

Transverse energy-energy correlations. Phys. Lett. B 750 427 (2015)

Summary of α_s measurements in jet physics

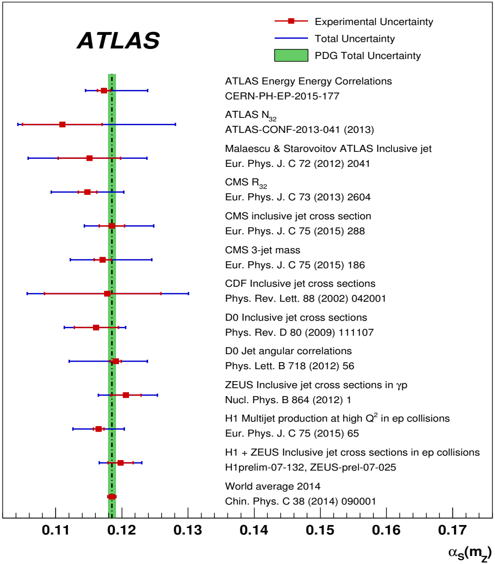

3. Photon measurements

Inclusive photons at $\sqrt{s} = 8$ TeV [JHEP 06, 005 (2016)]

- Photon phase space: $E_T^\gamma > 25$ GeV; $|\eta^\gamma| < 1.37$ or $1.56 < |\eta^\gamma| < 2.37$
- Cross-section measurement in four rapidity regions.
- NLO theoretical predictions by JetPhox
- NLO+NNNLL theoretical predictions by PeTeR (approx. NNLO)

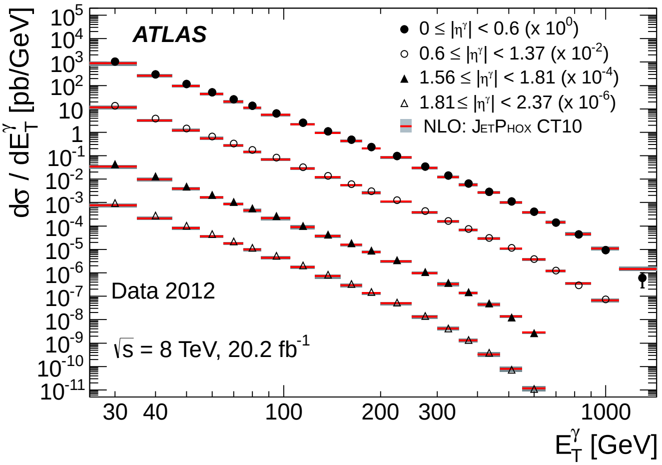

Systematics dominated by

- Background subtraction at low p_T
- Photon energy scale at high p_T

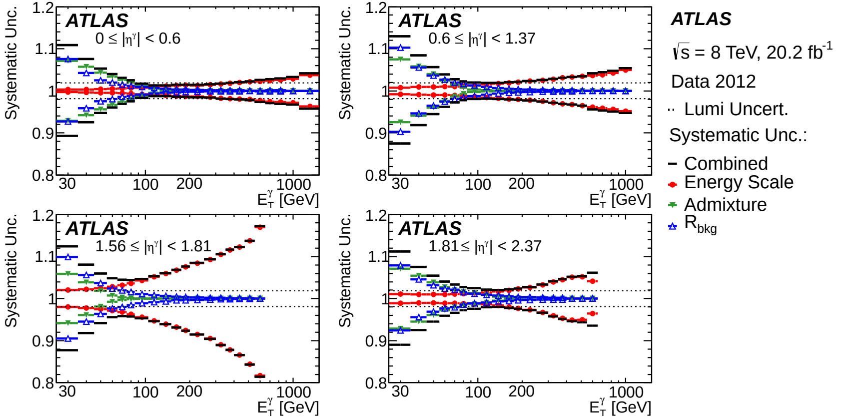

Ratios to NLO and NLO+NNNLL predictions

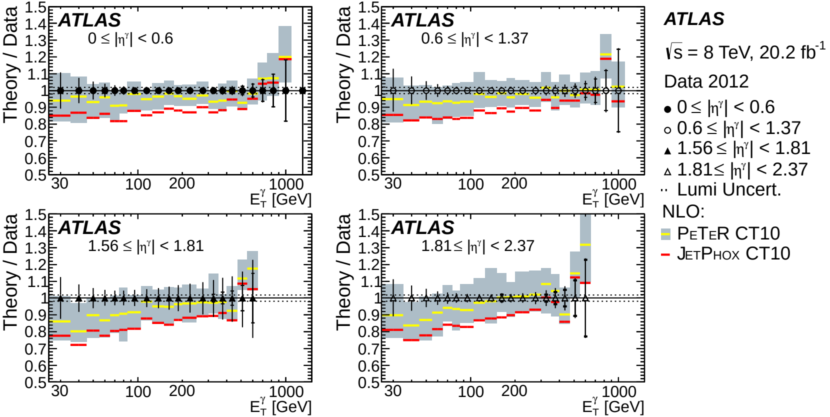

Ratios to LO+PS Monte Carlo expectations

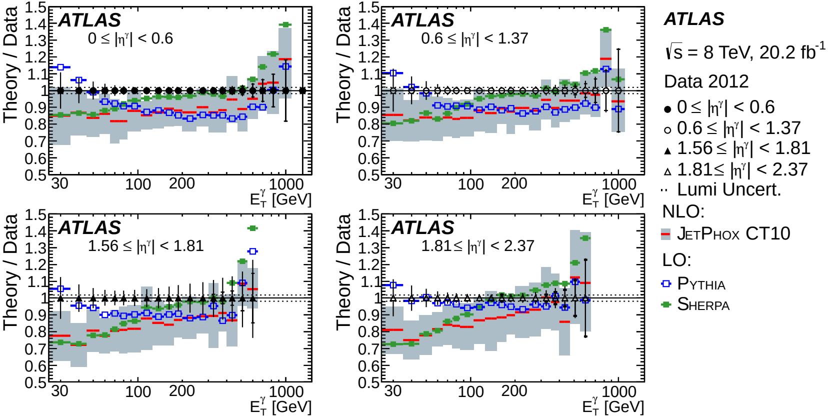

- $E_{T1}^{\gamma} > 25$ GeV and $E_{T2}^{\gamma} > 22$ GeV. $|\eta| < 1.37$ or $1.52 < |\eta| < 2.37$.
- Diphoton purities determined from a 2-dimensional fit to the isolation distributions of the two photons, with $\Delta R_{\gamma\gamma} > 0.4$

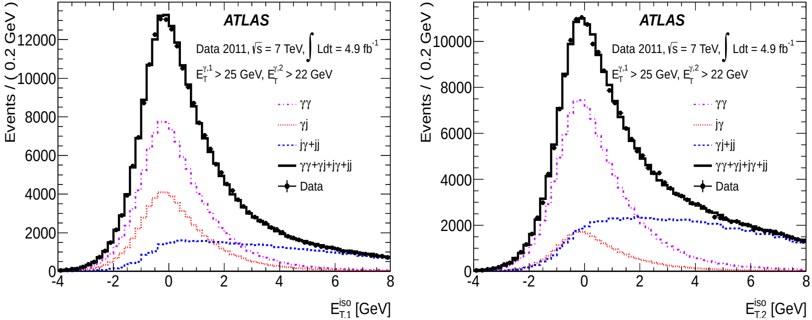

Yield	two-dimensional sidebands results			two-dimensional fit results		
$N_{\gamma\gamma}$	113 200	±600 (stat.)	${}^{+5000}_{-8000}$ (syst.)	111 700	±500 (stat.)	${}^{+4500}_{-7600}$ (syst.)
$N_{\gamma \mathrm{j}}$	31 500	±400 (stat.)	${}^{+3900}_{-3100}$ (syst.)	31 500	±300 (stat.)	${}^{+4800}_{-3600}$ (syst.)
$N_{\mathrm{j}\gamma}$	13 000	±300 (stat.)	${}^{+2500}_{-\ 800}$ (syst.)	13 900	${}^{+300}_{-200}$ (stat.)	${}^{+3400}_{-2100}$ (syst.)
N_{jj}	8 100	±100 (stat.)	${}^{+1900}_{-1400}$ (syst.)	8 300	±100 (stat.)	${}^{+\ 300}_{-2100}$ (syst.)

Event-by-event yields as a function of $m_{\gamma\gamma}$, $p_{T\gamma\gamma}$, $\Delta\phi_{\gamma\gamma}$ and $\cos\theta^*_{\gamma\gamma}$

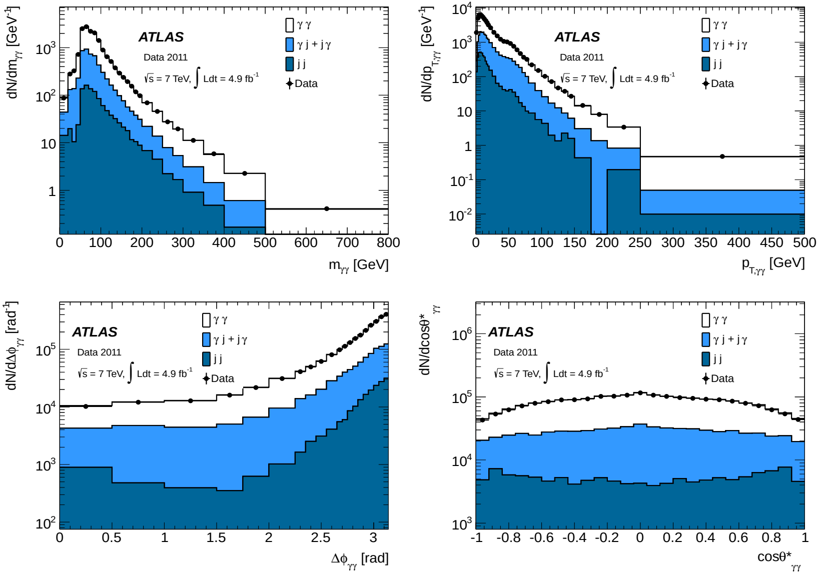

Corrected cross sections as a function of $m_{\gamma\gamma}$ and $p_{T\gamma\gamma}$

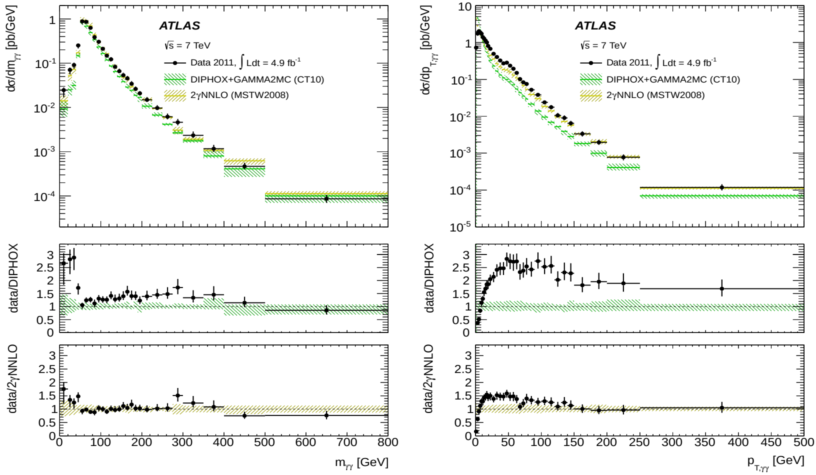

Comparison to DIPHOX and 2γNNLO. The latter provides better description.

Corrected cross sections as a function of $\Delta\phi_{\gamma\gamma}$ and $\cos\theta^*_{\gamma\gamma}$

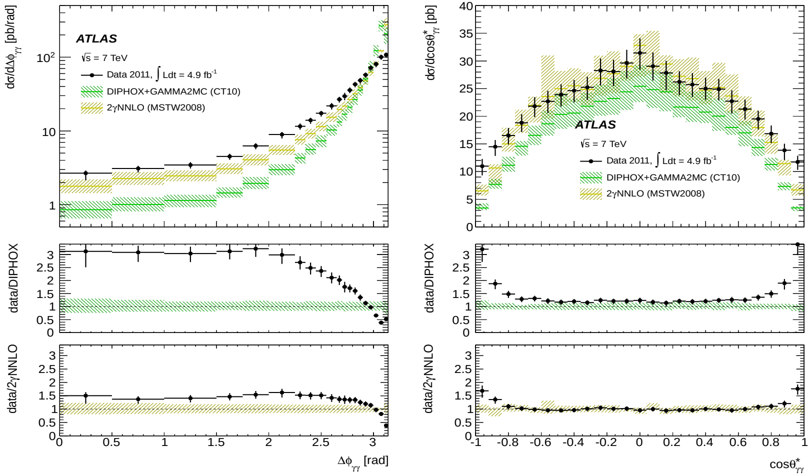

Comparison to DIPHOX and 2γNNLO. The latter provides better description.

- Photon phase space: $E_T^\gamma > 45$ GeV, $|\eta^\gamma| < 1.37$ or $1.52 < |\eta^\gamma| < 2.37$.
- Jet phase space: $p_T^j > 40$ GeV, $|y^j| < 2.37$, $\Delta R_{\gamma j} > 1$.
- $m_{\gamma j}$ and $\cos\theta_{\gamma j}$ measured for $|\eta^\gamma + y_j| < 2.37$, $|\cos\theta^{\gamma j}| < 0.83$ and $m_{\gamma j} > 161$ GeV.

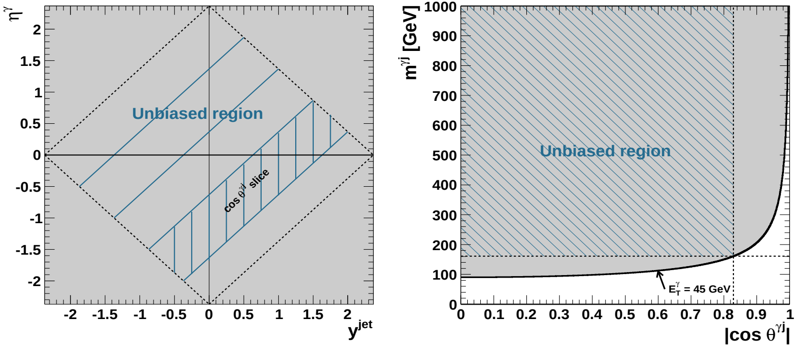

- Triangular cuts avoid biases on distributions affected by E_T^γ requirements.
- $\cos\theta^{\gamma j}$ sensitive to the spin of the particle in the propagator.

Dynamics of isolated photon + jet [Nucl. Phys. B 875, 483 (2013)]

Kinematical variables of the photon and the jet

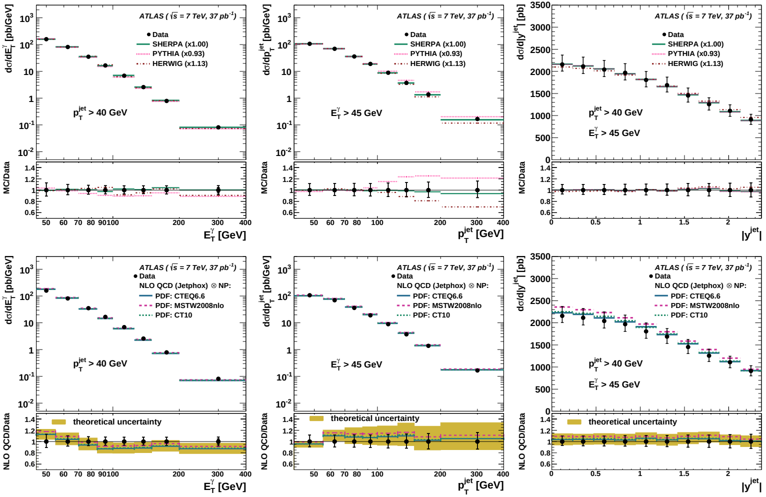

- SHERPA provides an excellent description
- Good agreement with NLO pQCD calculations

Dynamics of isolated photon + jet [Nucl. Phys. B 875, 483 (2013)]

Properties of the γ+jet system

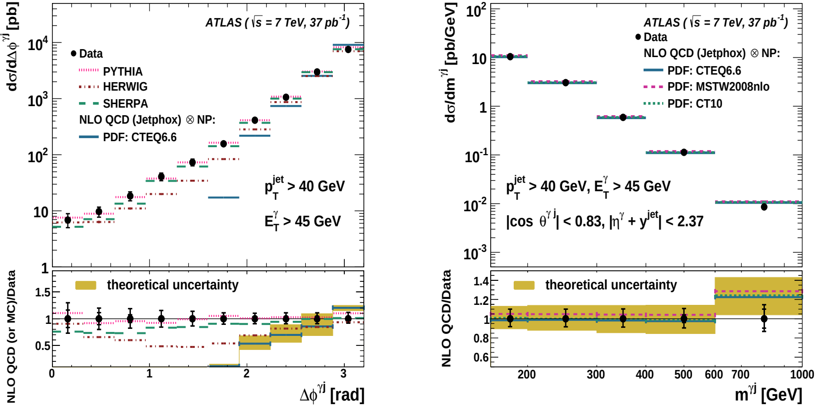

- $\Delta\phi_{\gamma j}$ not well described at NLO. LO+PS gives a good description.
- Need higher orders to fully describe azimuthal decorrelation.
- $m_{\gamma j}$ well described by NLO pQCD.

Angle between jet and photon in the centre-of-mass frame

$$\cos\theta_{\gamma j} \equiv \tanh\left(\frac{\Delta y_{\gamma j}}{2}\right)$$

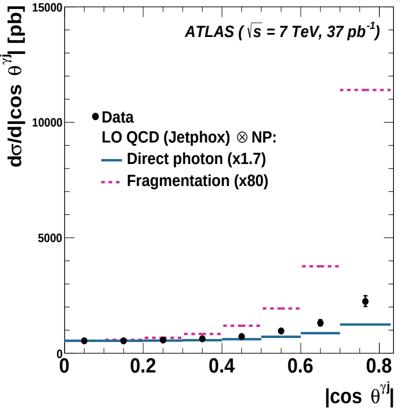

Sensitivity to the t-channel propagator

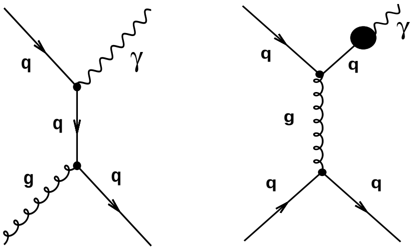

- Direct photon $\sim (1 - |\cos\theta^*|)^{-1}$
- Fragmentation $\sim (1 - |\cos\theta^*|)^{-2}$

- $\cos\theta_{\gamma j}$ is largely biased by the selection cuts.
- Unbiased shape recovered using triangular cuts described before.

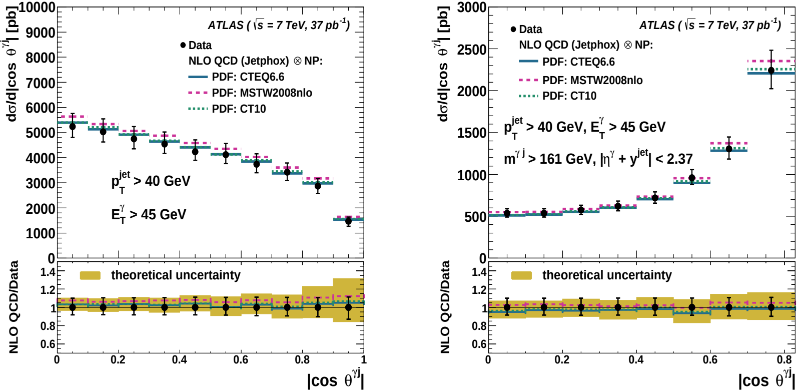

Conclusions

- A wide variety QCD phenomena has been explored at ATLAS using jets and photons.
- Several jet cross-sections have been measured to a high precision for large energy ranges.
- Limiting factor for jet measurements is the theoretical precision. Still dominated by scale uncertainty.
- Jet substructure variables provide insight on the current parton shower models.
- α_s measured to a very high experimental precision using TEEC.
- Several photon cross-section measured, show good overall agreement with theoretical predictions
- Many more measurements coming soon. Stay tuned!